THE AMERICAN SOCIETY OF MECHANICAL ENGINEERS
345 E. 47 St., New York, N.Y. 10017

86-GT-185

Production and Development of Secondary Flows and Losses Within Two Types of Straight Turbine Cascades

Part 2: A Rotor Case

A. YAMAMOTO
National Aerospace Laboratory
Chofu, Tokyo, Japan

ABSTRACT

Part 1 of this paper[1] presented the detailed mechanism of secondary flows and the associated losses occurring within a straight stator cascade with a relatively low turning angle of about 65°. Significant contribution of secondary flows on the loss production process was shown only near the blade suction surface downstream from the cascade throat (Z/Cax=0.74) in which region flows decelerated due to adverse pressure gradient.

In the second part, the same experimental analysis was applied to a straight rotor cascade with a much larger turning-angle of 102°. Flow surveys were made at twelve traverse planes located throughout the rotor cascade. The larger turning results in a similar but much stronger contribution of the secondary flows on the loss developing mechanism. Evolution of overall loss starts quite early within the cascade, and the rate of the loss growth is much larger in the rotor case than in the stator case.

NOMENCLATURE

A : Control area for calculating mass-averaged value
Cax : Cascade axial chord
CPs : Static pressure coefficient based on outlet velocity
CPt : Total pressure loss coefficient based on outlet velocity
CPt,1 : Total pressure loss coefficient based on inlet velocity
Csk : Secondary kinetic energy coefficient, $Csk=(Vs/\bar{V}m,12)^2$
H : Blade span
L.E. : Blade leading-edge
Patm : Atmospheric pressure
Ps : Static pressure
Pt : Total pressure
P.S. : Blade pressure surface
S.S. : Blade suction surface
T.E. : Blade trailing-edge
Vm : Resultant flow velocity
Vs : Magnitude of secondary flow vector
Vz : Axial velocity
Z : Axial distance from blade leading-edge
Y : Spanwise distance from hub endwall
δ_{99} : Boundary layer thickness
δ^* : Displacement thickness,

$$\delta^* = \int_0^{H/2} (1-\bar{V}m/\bar{V}m,mid)dY$$

Δ : Interval of contour plot
φ : represents θy, Vm, CPt, Vs or Csk
ρ : Density
δ^{**} : Momentum thickness,

$$\delta^{**} = \int_0^{H/2} (1-\bar{V}m/\bar{V}m,mid)(\bar{V}m/\bar{V}m,mid)dY$$

θy : Yaw flow angle measured from cascade axial direction

(Subscripts)
1-12 : indicate no. of traverse measuring (S3) planes
i : indicates pitchwise number of control areas in one blade pitch
j : indicates spanwise number of control areas in the whole span
mid : indicates mid-span

(Superscripts)
- : indicates pitchwise mass-averaged value
= : indicates overall mass-averaged value

INTRODUCTION

As clearly shown by Smith [2] in his experimental correlation between stage loading coefficients, flow coefficients and turbine efficiencies based on a number of expermental data of real turbines, the level of turbine efficiencies depends strongly on the loading coefficients; the efficiency tends to decrease with increase of the loading. The cascade turning-angle relates to the blade loading and is one of the main factors affecting the loss developing mechanism.

In this part of the paper, mechanism occurring within

Presented at the International Gas Turbine Conference and Exhibit
Dusseldorf, West Germany—June 8-12, 1986

a straight rotor cascade with a larger turning-angle than that in Part 1 will be made clear.

TEST CASCADE AND TEST CONDITION

Most of the test facilities is the same as described in Part 1 and only major differences are given here.

Low-Speed Straight Turbine Rotor Cascade

The blade profile is the same as the MEAN profile of the first stage high pressure turbine rotor for aeroengine use[3] and is given in the appendix. The major specifications of the cascade are as follows;

-- Blade chord, C = 73.5 mm
-- Axial blade chord, Cax = 72.6 mm
-- Blade pitch, S = 61.42 mm
-- Aspect ratio, H/C = 1.37
-- Solidity, S/C = 1.36
-- Number of blades, N = 6
-- Cascade inlet angle(at design), $\theta y,inlet = 49.8^{\circ}$
-- Cascade outlet angle(at design), $\theta y,outlet = -63.5^{\circ}$
-- Turning angle(at design) $= 113.3^{\circ}$

It is characterized by thick leading and trailing-edges, low aspect-ratio and low solidity for air-cooling, and by a large turning-angle for large loading. The present rotor blades were made of aluminium material by a wire-cutting manufacturing method. The test cascade is shown in Photo 1. In the present case of the rotor cascade, two sheets of about 12mm-wide x 0.1mm-thick alminium film are adhered on the blade surfaces near the tip. The purpose is the same as described in Part 1.

Test Condition

Twelve measuring planes analyzed in the paper are shown in Fig.1. The test Reynolds number, based on the mass-averaged outlet velocity at the furthest downstream traverse plane (plane 12,Z/Cax=1.23) and the blade chord, was about 1.8×10^5. Turbulence intensity of the inlet free stream obtained at plane 1 was about 0.5%.

In the present test, differences between the design and the test flow angles are as follows;

	Design	Test
-- Inlet flow angle	49.8°	40.1° ($i=-9.7^{\circ}$ at plane1)
-- Outlet flow angle	-63.5°	-61.7°
-- Turning angle	113.3°	101.8°.

The inlet flow conditions and the inlet inlet endwall boundary layer parameters are as follows;

-- Density, $\rho=1.22 kg/m^3$, Viscosity, $\nu=1.44 \times 10^{-5} m^2/s$
-- $\bar{\bar{V}}m,1=23.9$ m/s, $\bar{\bar{V}}m,1,mid=24.6$ m/s, $\bar{\bar{V}}m,12=35.3$ m/s
-- Turbulence intensity in free stream, Tu,1=0.5 %

	Hub	Tip
-- Boundary layer thickness, δ_{99}/H =	0.117	0.105
-- Displacement thickness, δ^*/H =	0.0132	0.0266
-- Momentum thickness, δ^{**}/H =	0.0094	0.0152
-- Shape factor, δ^*/δ^{**} =	1.41	1.75

The above boundary layer parameters were calculated from the spanwise distribution of the pitchwise mass-averaged resultant velocity at the cascade inlet plane 1 (i.e., Z/Cax=-0.26 in Fig.5).

ANALYSIS METHOD

Secondary flow vectors (Vs) were obtained in the same manner given in Part 1. The secondary flow velocities (Vs) were normalized by the mass-averaged flow velocity at plane 12, i.e., $\bar{\bar{V}}m,12$ at Z/Cax=1.23. The normilized vectors were drawn by looking at them from the downstream side of the cascade. The secondary kinetic

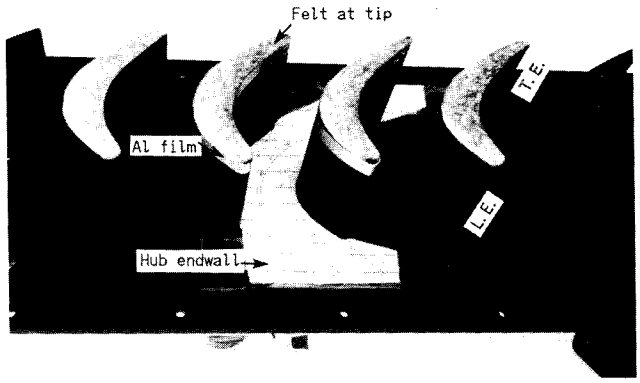

Photo 1 Test cascade (rotor case)

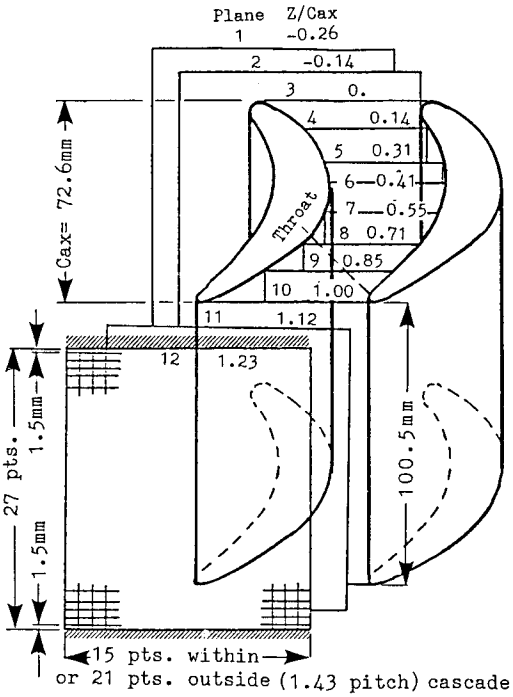

Fig.1 Traverse measuring planes of straight rotor cascade (S3 Planes)

energy coefficients (Csk) is calculated by

$$Csk = (Vs/\bar{\bar{V}}m,12)^2 \quad \text{and} \quad Csk,1 = (Vs/\bar{\bar{V}}m,1)^2$$

Total pressures (Pt) were normalized in the form of total pressure loss coefficients by

$$CPt = (Patm - Pt)/(0.5 \times \rho \times \bar{\bar{V}}m,12^2)$$

and

$$CPt,1 = (Patm-Pt)/(0.5 \times \rho \times \bar{\bar{V}}m,1^2)$$

where Patm is the atmospheric pressure and ρ is density. $\bar{\bar{V}}m,12$ and $\bar{\bar{V}}m,1$ are the mass-averaged cascade outlet velocity at plane 12 and the mass-averaged inlet velocty at plane 1.

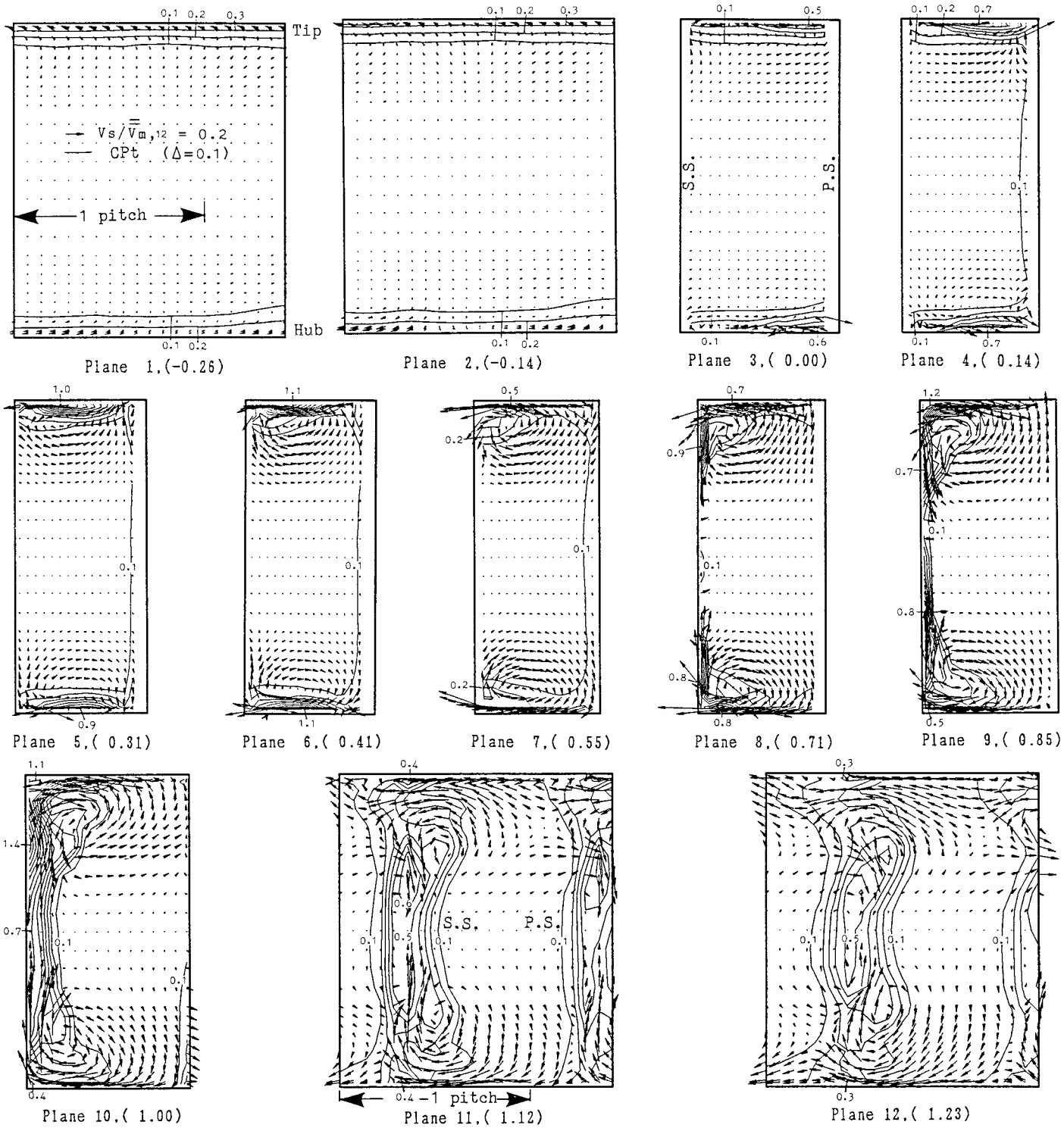

Fig.2 Development of Secondary flows and total pressure losses before,within and after a straight rotor cascade ,S3 Planes,(Z/Cax)

Similarly, static pressure (Ps) is normalized by

$$CPs = (Ps - Patm)/(0.5 \times \rho \times \bar{\bar{V}}m,12^2).$$

The mass-averaging procedure for yaw flow angle, resultant velocity and loss coefficient is given in Part 1. The definition of S1, S2 and S3 planes are also given in Part 1 and a sketch of them is given in Fig.3 of the present paper.

EXPERIMENTAL RESULTS AND DISCUSSION

Secondary Flows and Total Pressure Losses at Traverse Planes (S3 Planes, Fig.2)

Fig.2 represents a process of production and development of secondary flows and the associated losses through the cascade. Note that the scale of the secondary flow vector adopted in this figure is shortened to half the scale adopted in Part 1, since the magnitude of secondary flows are generally too large to plot without confusing the vectors with the contours of CPt.

In the present case with larger turning, the loss production mechanism due to secondary flows is essentially the same as that seen in Part 1, except the following: The counter vortex at the suction surface(S.S.)/endwall corner can be clearly seen only at plane 3 (Z/Cax=0.0) which corresponds to just the cascade inlet plane. Gregory-Smith and Graves[4] measured this vortex also at Z/Cax=0.03 of their straight rotor cascade. In the following discussion, a number included in a bracket following a plane number represents the value of Z/Cax, i.e., normalized axial distance from the blade leading-edge. The vortex has almost disappeared at the next downstream plane, plane 4 (0.14). Passage votices have already fully developed at plane 5 (0.31). Rolling-up of low-energy fluids onto the S.S. has started at plane 7 (0.55) which is yet located upstream of the cascade throat. The passage vortices are very strong and they concentrate low-energy fluids in very thin loss-cores on the S.S., as seen typically at plane 8 (0.71). The spanwise flows of the low-energy fluids comming from the both endwalls meet together at plane 9 (0.85). They rapidly increase the thickness of the high-loss region on the S.S. after the meeting, as seen at plane 10 (1.00). It should be noted that the secondary flow vectors at plane 7 show very smooth circulation and are not so disturbed even at the S.S./endwall corner ,while those at planes 6 and 8 show irregular vector plots. This will be discussed later on the loss distribution near the endwalls.

Downstream from the cascade, i.e., at plane 11 and 12, the strong rolling-up of the passage vortices promote the fluid mixing and energize the wake flow especially from the endwall sides. These downstream vector plots represent quite similar patterns of secondary flow field shown in Fig.2 of Sieverding's paper [5], which figure was cited from Armstrong's paper[6]; the figure presents blade shed circulation in addition to passage vortex, as shown here.

The distance of the passage vortex center from the endwall is constant only up to plane 9 (0.85) and increases at the downstream planes in the present rotor cascade, while the distance was always constant in the stator cascade.

Static Pressure Distribution on S1, S2 and S3 Planes (Fig.3)

The two S1 (blade-to-blade) planes shown in Fig.3 correspond to the planes located apart from the hub endwall by 1.48 % and 50 % of the span height. The difference between the two static pressure distributions on these two S1 planes is more significant in the present rotor case than in the stator case. The minimum pressure points on both planes are located apart from the S.S. in the present cascade, too. The distance between these two minimum pressure points is larger in the present case. The point on the mid-span S1 plane is located farther upstream and closer to the S.S. than that on the S1 plane near the endwall.

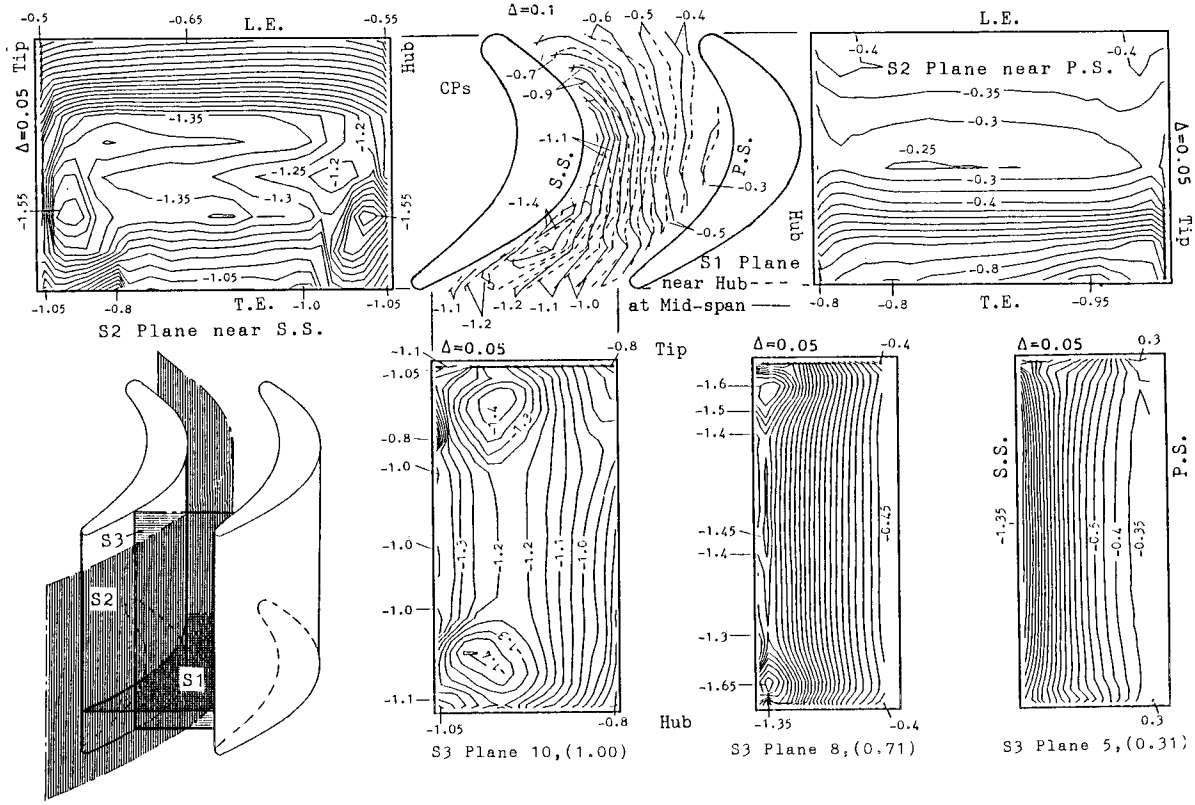

Fig.3 Static pressure distribution on various planes within a rotor cascade

The static pressure contours on the S2 surface near the P.S. reveals a fairly large deceleration region located between the leading-edge and the half axial chord. Especially at the P.S./endwall corners near the leading-edge, the rate of flow decelaration is large. As already seen in Fig.1, the inlet flows near the corners were moving toward the endwalls. Similar corner flows in the regions may be found in Fig.20 of Gregory-Smith and Graves[4] of their measurements by a pitot tube, and also in Fig.5(g) of Marchal and Sieverding[7] of pressure surface flow visualization of their rotor cascade.

Static pressure contours on the S2 surface near the S.S. reveal that there is a fairly large region with almost constant pressure and with adverse pressure gradient (flow deceleration) between the 1/3 axial chord and the trailing-edge. Near both endwall corners in this region, strong effects on the pressure field due to the passage vortices can be seen.

Three figures obtained at S3 planes show the effects on the pressure field within the cascade. Significant effects start to appear at plane 8 (0.71).

Total Pressure Distribution on S1, S2 and S3 Planes within Rotor Cascade (Fig.4)

The loss distribution on the S1 (blade-to-blade) plane near the hub endwall has two local maximum peaks in the present case too as seen in Part 1. The locations of the peaks, however, are different from those in the stator case; one is located farther inside the cascade. The peak loss value is very large. The other is located near the S.S. (not on the S.S. as in Part 1) just at the cascade throat. These endwall loss contours may relate to endwall shear stress contours. Gaugler and Russel[8], for example, give a figure of endwall shear stress contours within a straight turbine stator cascade with a turning-angle of 72°; the shear stress contours were obtained by manually sketching the contours of constant relative motion of a number of oil drops taken by movie camera. Their result also presents two local maximum peaks within the cascade; one is located at about half axial-chord from the cascade inlet (i.e., a little closer to the S.S. than one of the present loss peaks), and the other is located on the S.S. downstream from the throat in their case. Further detailed comparison, however, can not be made at present. The figure also indicates that the S.S./endwall corner along the S.S. is dominated by lower loss compared to the neighboring region.

Contours of CPt on the S2 plane near the P.S. show higher loss near the P.S. in the rotor case than in the stator case. This is due to the flow deceleration over the P.S. as was seen in Fig.3. The largest loss values near the P.S. can be found at the leading-edge/endwall corners where the flows were much decelerated and were moving toward the endwalls. Another S2 contour plot obtained near the S.S. indicates significant accumulation of low-energy fluids over a large area of the S.S. downstream from the throat. A large part of the loss is apparently produced in the flow deceleration regions where the directions of both pressure force and shear force are opposite each other.

Contour plots at several S3 planes clearly show the migration process of the cascade inlet boundary layers onto the S.S. See especially the movement of the maximum loss values along the endwalls. It is noteworthy that the maximum losses on the endwalls decrease once at plane 7(0.55) and increase again at plane 8(0.71). This can be seen also on the S1 plane previously discussed. The decrease at plane 7 coincides

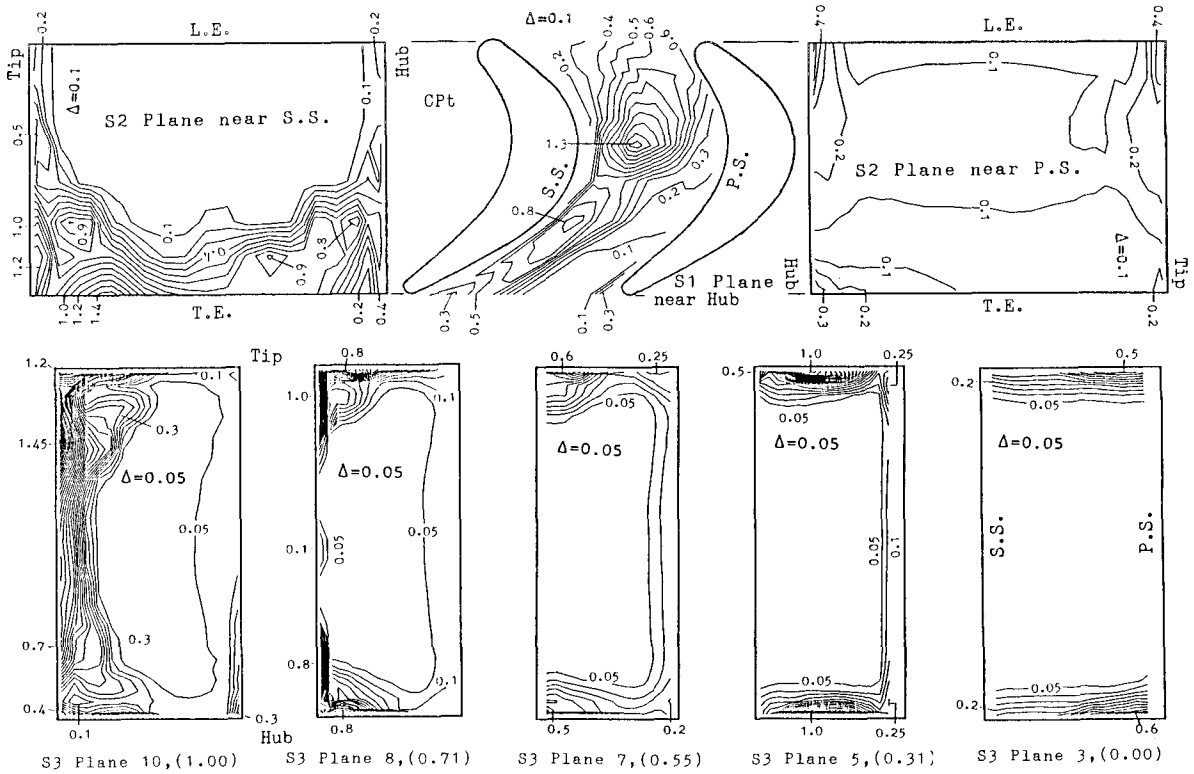

Fig.4 Total pressure loss distribution on various planes within a rotor cascade

with the disappearance of irregular vector plots of the passage vortices at the S.S./endwall corner, as was seen in Fig.2.

Spanwise Distribution of Pitchwise Mass-Averaged Yaw Angle, Velocity and Loss through Rotor Cascade (Fig.5)

The difference between the two yaw angles at plane 1 and at plane 12 indicates that the mass-averaged turning-angle in the present test is about 102°.

Every curve of yaw angle distribution downstream from plane 5 has two local maximum values (under-turning compared to the mid-span flow direction), two minimum values (over-turning), and two increased values near the endwalls. The first two and the second two values result from the effects of the passage vortices. The increased values near the walls are probably caused by the wall shear stresses which draw back the over-turning flows in the under-turning direction. The shear forces may generate corner vortices at the S.S./endwall corner. Sieverding[5] describes that this kind of underturning shows the existence of corner vortex in the corner. The present plots of secondary flow vectors shown in Fig.2, however, did not represent any clear circulation of flows near the endwalls, although clear underturning of the flows could be detected in the mass-averaged values. A more detailed survey of the flow near the endwall is

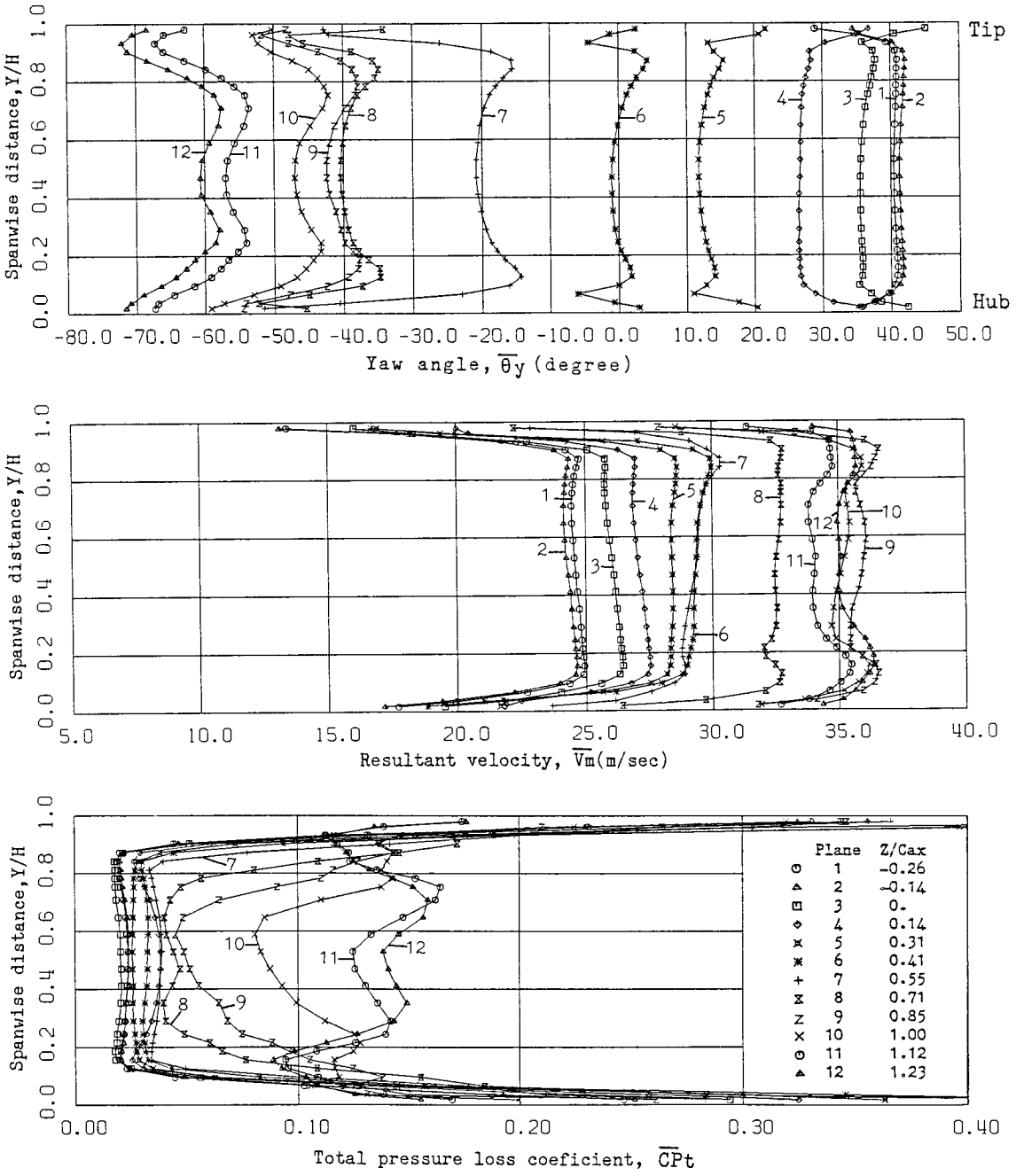

Fig.5 Spanwise distribution of pitchwise-averaged yaw flow angle, resultant velocity and total pressure loss coefficient

needed.

The figure of the resultant velocity shows that the mass-averaged acceleration ratio (i.e., $\overline{Vm}$,12/$\overline{Vm}$,1) is about 1.48, which indicates lower acceleration compared to the value of 2.78 of the stator. The thickness of the inlet boundary layer is about 0.11 of the cascade span height. Flows from plane 9 (0.85) to plane 11 (1.12) decelerate.

The loss curves in Fig.5 show the spanwise and streamwise development of the pitchwise mass-averaged loss through the cascade. The losses increase first near the endwall regions and finally along the whole span. Downstream from the cascade, i.e., planes 11 and 12, the rate of the loss growth decreases.

Evolution of Overall Total Pressure Loss through Rotor Cascade (Fig.6)

In the present rotor case with a large turning-angle, the curve of mass-averaged overall loss, as shown in Fig.5, starts to increase at Z/Cax=0.25 near the cascade inlet. The loss grows up steadily toward the downstream of the cascade, Z/Cax=1.23.

The mass-averaged loss at the mid-span also increases in parallel with the overall loss. The difference between the two loss values corresponds approximately to the secondary loss including the loss due to the endwall boundary layers within the cascade. Downstream from the trailing-edge, the mid-span loss increases more rapidly beyond the overall loss. This is because the migration of the low-energy fluids reach the mid-span of the wake due to the fluid mixing caused by the strong secondary flows (passage vortices).

The secondary kinetic energy coefficient starts to increase at the cascade inlet and rapidly increases from Z/Cax=0.25 up to the trailing-edge plane (Z/Cax=1.0). The coefficient, however, falls down abruptly downstream of the cascade.

Among the experimental results on the overall loss evolution reported so far, Langston et al.[9] and Gregory-Smith and Graves[4] indicated steady growth of the overall loss up to about Z/Cax=0.9 and then rapid growth downstream from there in their rotor cascades. Sieverding[5] showed no growth up to about Z/Cax=0.4 for an impulse rotor cascade and up to about Z/Cax=0.7 for both of their rotor and stator cascades. In the theoretical approach on the loss growth, Hah [10] predicted quite early start of the loss growth roughly located between Z/Cax=0.2 and 0.4, by full Navier Stokes(N.S.) equations with an algebraic Reynolds stress model for Langston's straight rotor cascade[9], while Moore and Moore[11] predicted slower loss growth by a fully elliptic N.S. code with the Prandtl mixing-length turbulence model and with an elliptic pressure-correction for the same cascade. The latter could predict the loss development of Langston et al.[9] better than the former. The tendency of the present result of CPt is similar to the Hah's predicted result although the present cascade geometry is different from that dealt with by Hah. The overall behavior of the present experimental Csk is very similar to that predicted by Moore and Moore.

CONCLUSIONS

The present study gave fairly detailed quantitative data on the secondary flow/loss mechanism in a straight rotor cascade with a larger turning-angle than that of the stator cascade described in Part 1. As expected, the present cascade caused more significant loss (CPt based on the outlet velocity) due to the stronger secondary flows occurring within the rotor cascade than within the stator cascade. The passage vortices, which

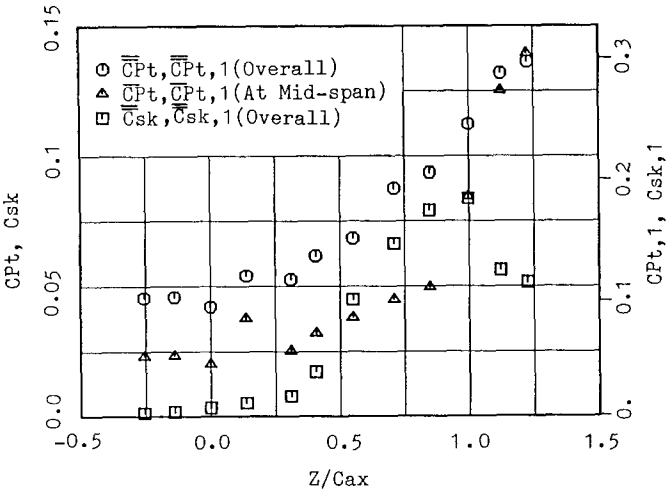

Fig.6 Evolution of mass-averaged total pressure loss (Straight rotor cascade)

were again the most important in the loss production process, started to grow at an early stage within the cascade. Larger turning of flow in the rotor cascade produced higher loss levels near the endwalls and near the blade surfaces. These lead to a rapid and steady growth of the overall loss from a near-inlet plane to the outlet plane of the cascade.

ACKNOWLEDGEMENTS

The authors wish to sincerely thank Mr. H. Nouse, Director of the Aeroengine Division, for his support of the present study and his helpfull discussion, Mr. H. Usui, a staff member of the Turbine Section for his assistance in the computational work, Mr. H. Tateishi, a staff member of Maruwa Electric Industry and Mr. H. Tamura, a student of Nihon University, for their assistance in the experimental work.

REFERENCES

1. Yamamoto,A.,"Production and Development of Secondary Flows and Losses within Two Types of Straight Turbine Cascades, Part 1: A Stator Case", to be presented at the 1986 ASME Gas Turbine Conference in Dusseldorf, 1986.

2. Smith,S.F.,"A Simple Correlation of Turbine Efficiency", Journal of the Royal Aeronautical Science, Vol.69, pp.467, 1965.

3. Yamamoto,A., Takahara,K, Nouse,H., Inoue,S., Usui,H., and Mimura,F., "An Aerodynamic Design and the Overall Stage Performance of an Air-Cooled Axial-Flow Turbine", National Aerospace Laboratory, TR-321T, Jan. 1981.

4. Gregory-Smith,D.G., and Graves,C.P., "Secondary Flows and Losses in a Turbine Cascade", Viscous Effects in Turbomachines, AGARD-CP-351, 1983.

5. Sieverding,C.H., "Recent Progress in the Understanding of Basic Aspects of Secondary Flows in Turbine Blade Passages", ASME paper No.84-GT-78, 1984.

6. Armstrong, W.D., "The Secondary Flow in a Cascade of Turbine Blades", ARC R.M 2979, 1955.

7. Marchal,P., and Sieverding,C.H., "Secondary Flows within Turbomachinery Bladings", Secondary Flows in Turbomachines, AGARD-CP-214, 1977.

8. Gaugler,R.E., and Russel,L.M., "Comparison of,Visualized Turbine Endwall Secondary Flows and Measured Heat Transfer Patterns", ASME paper No. 83-GT-83, 1983.

9. Langston,L.S., Nice,M.L., and Hooper,R.M., "Three Dimensional Flow within a Turbine Cascade Passage", ASME Journal of Engineering for Power, Vol.99, No.1, 1977, pp.21-28.

10. Hah,C.,"A Navier-Stokes Analysis of Three-Dimensional Turbulent Flows inside Turbine Blade Rows at Design and Off-Design Conditions", ASME paper No. 83-GT-40,1983.

11. Moore,J., and Moore,J.G., "Performance Evalution of Linear Turbine Cascade using Three-Dimensional Viscous Flow Calculations", ASME paper No. 85-GT-65,1985.

APPENDIX

Blade Profile Coordinates

(mm)

I	X	Yp	Ys
1	0.000	0.000	-6.329
2	4.083	0.817	-12.250
3	8.167	-2.001	-17.354
4	12.250	-4.614	-21.438
5	16.333	-6.533	-24.500
6	20.417	-7.963	-26.338
7	24.500	-8.657	-27.563
8	28.583	-8.657	-27.767
9	32.667	-8.085	-27.358
10	36.750	-6.860	-26.133
11	40.833	-4.900	-24.214
12	44.917	-2.654	-21.233
13	49.000	0.531	-18.171
14	53.083	4.288	-13.067
15	57.167	8.698	-7.350
16	61.250	13.271	-0.408
17	65.333	18.171	7.146
18	69.417	-	15.108

DL	(XL , YL)	DT	(XT , YT)
8.167	(2.654 , -3.063)	4.083	(69.090, 19.396)

Dmax	(Xmax , Ymax)	CHORD
18.906	(29.808 , -18.171)	73.5

where DL, DT and Dmax represent diameters of blade leading-edge, trailing-edge and blade maximum thickness, and CHORD represents blade chord length. The coordinate points were smoothly connected to make the blade profile.